Invasive breast carcinoma cells from patients exhibit Mena[superscript INV]- and macrophage-dependent transendothelial migration

Published in final edited form as:
Sci Signal. ; 7(353): ra112. doi:10.1126/scisignal.2005329.

Invasive breast carcinoma cells from patients exhibit Mena^{INV}- and macrophage-dependent transendothelial migration

Jeanine Pignatelli[1,*], **Sumanta Goswami**[1,2], **Joan G. Jones**[1,3,4,5], **Thomas E. Rohan**[3], **Evan Pieri**[2], **Xiaoming Chen**[1], **Esther Adler**[4], **Dianne Cox**[1], **Sara Maleki**[4], **Anne Bresnick**[6], **Frank B. Gertler**[7], **John S. Condeelis**[1,5,8,*], and **Maja H. Oktay**[4,*]

[1]Department of Anatomy and Structural Biology, Albert Einstein College of Medicine, Bronx, NY 10461, USA

[2]Department of Biology, Yeshiva University, New York, NY 10033, USA

[3]Department of Epidemiology and Population Health, Albert Einstein College of Medicine, Bronx, NY 10461, USA

[4]Department of Pathology, Albert Einstein College of Medicine/Montefiore Medical Center, Bronx, NY 10467, USA

[5]Integrated Imaging Program, Albert Einstein College of Medicine, Bronx, NY 10461, USA

[6]Department of Biochemistry, Albert Einstein College of Medicine, Bronx, NY 10461, USA

[7]David H. Koch Institute for Integrative Cancer Research, Massachusetts Institute of Technology, Cambridge, MA 02139, USA

[*]Corresponding authors: moktay@montefiore.org (M.H.O.); jeanine.pignatelli@einstein.yu.edu (J.P.); john.condeelis@einstein.yu.edu (J.S.C.).

SUPPLEMENTARY MATERIALS
www.sciencesignaling.org/cgi/content/full/7/353/ra112/DC1
Fig. S1. The experimental setup of the iTEM assay and the permeability of HMEC endothelium.
Fig. S2. TMEM score and relative Mena^{INV} abundance in LN-positive or LN-negative cases.
Fig. S3. iTEM assays engineered with HMEC-1 endothelium performed with human IDC cells obtained by FNA.
Table S1. *MENA* and *GAPDH* primer sequences.
Table S2. Correlation coefficients for TMEM score and relative expression of *MENA* isoforms in IDCs, overall and by clinical subtype.
Table S3. TMEM scores and relative Mena isoform expression for tumors with different clinical and pathological variables.
Table S4. Clinical and pathological data pertaining to iTEM data in fig. S3A.
Table S5. Clinical and pathological data pertaining to iTEM data in Figs. 4 and 6.

Author contributions: J.P. performed qPCR analysis, developed and performed the iTEM assay, immunofluorescence, xenographs, mouse FNA, siRNA, data analysis, and statistics, and contributed to the experimental design and wrote the manuscript. S.G. performed qPCR and data analyses, and contributed to the experimental design and manuscript editing. J.G.J. performed IHC and TMEM scoring. T.E.R. performed the statistical analysis of patient samples. E.P. performed qPCR analysis. X.C. and E.A. collected patient FNA samples. D.C. differentiated the primary macrophages. S.M. performed E-cadherin scoring. A.B. developed the iTEM assay. F.B.G. developed the Mena antibody. J.S.C. contributed to the experimental design, data analysis, and wrote the manuscript. M.H.O. performed IHC, TMEM, and E-cadherin scoring, statistics, and data analysis, and contributed to the experimental design and wrote the manuscript.

Competing interests: T.E.R., J.G.J., J.S.C., and F.B.G. hold stock and/or equity in MetaStat Inc. T.E.R. and J.G.J. have received consulting fees from MetaStat Inc. J.G.J. was a member of MetaStat's Clinical Advisory Board. All other authors declare that they have no competing interests.

Data and materials availability: J.S.C., S.G., and F.B.G. hold a patent pertaining to the use of Mena^{INV} in cancer diagnosis, prognosis, and treatment (U.S. Patent 8603738). J.S.C., T.E.R., F.B.G., and J.G.J. hold a patent for the TMEM-based MetaSite Breast diagnostic assay (8642277).

[8]Gruss Lipper Biophotonics Center, Albert Einstein College of Medicine, Bronx, NY 10461, USA

Abstract

Metastasis is a complex, multistep process of cancer progression that has few treatment options. A critical event is the invasion of cancer cells into blood vessels (intravasation), through which cancer cells disseminate to distant organs. Breast cancer cells with increased abundance of Mena [an epidermal growth factor (EGF)–responsive cell migration protein] are present with macrophages at sites of intravasation, called TMEM sites (for tumor microenvironment of metastasis), in patient tumor samples. Furthermore, the density of these intravasation sites correlates with metastatic risk in patients. We found that intravasation of breast cancer cells may be prevented by blocking the signaling between cancer cells and macrophages. We obtained invasive breast ductal carcinoma cells of various subtypes by fine-needle aspiration (FNA) biopsies from patients and found that, in an in vitro transendothelial migration assay, cells that migrated through a layer of human endothelial cells were enriched for the transcript encoding $Mena^{INV}$, an invasive isoform of Mena. This enhanced transendothelial migration required macrophages and occurred with all of the breast cancer subtypes. Using mouse macrophages and the human cancer cells from the FNAs, we identified paracrine and autocrine activation of colony-stimulating factor-1 receptor (CSF-1R). The paracrine or autocrine nature of the signal depended on the breast cancer cell subtype. Knocking down $Mena^{INV}$ or adding an antibody that blocks CSF-1R function prevented transendothelial migration. Our findings indicate that $Mena^{INV}$ and TMEM frequency are correlated prognostic markers and CSF-1 and $Mena^{INV}$ may be therapeutic targets to prevent metastasis of multiple breast cancer subtypes.

INTRODUCTION

Metastasis is a complex multistep process that involves cancer cell dissemination and, ultimately, patient death (1). The outcome of breast cancer patients with metastatic disease has not improved in the past 30 years in spite of the development of targeted therapies (2). Thus, understanding the details of the metastatic process is of paramount importance for the development of new prognostic and therapeutic targets.

Intravital imaging in animal models has revealed many aspects of metastasis (3–6), including the essential roles that macrophages play in the micro-environments in which mammary tumor cells invade, migrate, and intravasate (5, 7). In particular, intravital imaging of rodent mammary tumors shows that breast cancers contain a subpopulation of highly motile cancer cells that move alongside macrophages in streams toward blood vessels in response to para-crine chemotactic signaling (6, 8, 9). Upon reaching a blood vessel, cancer cells intravasate at sites enriched with perivascular macrophages (5).

Expression profiling of the invasive subpopulation of cancer cells obtained from primary tumors revealed changes in the expression of genes associated with motility pathways that control actin polymerization, epidermal growth factor (EGF)–directed cell movement, and invadopodium formation (10, 11). Directed migration of various cells is typically initiated by chemo-tactic signaling, which induces cytoskeletal rearrangements involving cofilin (12–14). Mena, a member of Ena/VASP family of actin-binding proteins, is a key mediator of

cytoskeletal arrangement and functions at the convergence of the cofilin-regulated motility pathways (15, 16). Mena enhances tumor cell migration toward EGF in vivo in part by interfering with the activity of inhibitory capping proteins and increasing actin filament elongation rates, thereby promoting actin polymerization (6, 16, 17). These activities are essential for sustained directional cell movement in response togrowth factors like EGF (18).

In patients, *MENA* expression is increased in precursor lesions of the cervix and colon, in breast lesions associated with high risk of cancer development, and in high-grade primary and metastatic breast tumors (19). Three Mena protein isoforms arising from alternative splicing are particularly important in human breast cancer: $Mena^{classic}$, $Mena^{INV}$, and Mena11a. $Mena^{classic}$ contains only the constitutive exons, whereas the two splicevariants $Mena^{INV}$ and Mena11a contain alternatively included exons termed “INV” or “11a,” respectively. The INV (also known as “+++”) exon encodes a 19–amino acid residue inserted near the N terminus, whereas the 11a exon encodes a 21–amino acid residue inserted near the C terminus (11, 17, 20). $Mena^{INV}$ abundance potentiates chemotactic and invasive responses of carcinoma cells to EGF (6, 16). The observed increase in *MENA* expression in invasive and disseminating tumor cells reflects increased abundance of both $Mena^{classic}$ and $Mena^{INV}$, and correlates with decreased Mena11a abundance relative to that observed in noninvasive, nonintravasating tumor cells within primary mammary tumors(17).Mena forms tetramers via a C-terminal coiled-coil sequence that is conserved in all Ena/VASP proteins, and $Mena^{classic}$ and $Mena^{INV}$ are thought to form $Mena^{classic}$/ $Mena^{INV}$ heterotetramers (11, 21).

MENA expression is found in cancer cells located at the micro-anatomical sites of cancer cell intravasation, called TMEM (tumor micro-environment of metastasis) sites (22, 23). These sites, initially observed by intravital imaging of rodent mammary tumors, have also been detected in human invasive ductal carcinomas (IDCs) by triple immunohistochemistry (IHC) (22). A TMEM site is defined as a *MENA*-expressing tumor cell that is in direct contact with an endothelial cell and a perivascular macrophage. Case-control studies show that the number of TMEM sites is associated with increased risk of developing distant metastases in patients with IDC of the breast (22, 23). IDC sampled by fine-needle aspiration (FNA) biopsies indicates that the relative abundance of $Mena^{INV}$ correlates with TMEM frequency, stability, and/or function in patients (14). Increased $Mena^{INV}$ abundance increases transendothelial migration (TEM) in cultured cells and promotes cell migration, streaming, intravasation, and formation of spontaneous lung metastases in orthotopic xenografts in mice (6). Other studies show that *Mena* knockout mice bred with PyMT (polyoma virus middle T antigen) transgenic mice develop tumors with reduced intravasation and metastasis and have prolonged survival (24). Thus, $Mena^{classic}$ and/or $Mena^{INV}$ may promote metastasis by inducing TEM activity during intravasation.

Here, we tested the hypothesis that the $Mena^{INV}$ isoform in particular is linked to TMEM score and the associated TEM at these proposed sites of intravasation (14, 25) by measuring the TEM activity of primary tumor cells from patients using new in vitro assays.

RESULTS

Mena^{INV} transcript expression positively correlates with the number of TMEM intravasation sites

Our previous study showed a positive correlation between Mena^{INV} and TMEM scores in a cohort of 40 IDCs of the breast obtained from patients, indicating that relative Mena^{INV} abundance correlates with epithelial disco-hesion and TMEM score in breast cancer patients (14). Here, we wanted to confirm this correlation in a larger patient cohort. We measured the abundance of transcripts encoding Mena^{INV} and Mena11a by quantitative real-time polymerase chain reaction (qRT-PCR) in FNA samples from IDCs in a cohort of 60 patients and determined TMEM scores in formalin-fixed, paraffin-embedded (FFPE) breast cancer tissue by triple IHC from the same cohort of 60 patients (Fig. 1A). We previously demonstrated that quantification of the Mena isoforms by immunoblotting is not precise enough for correlation analysis with the TMEM score because of the lack of antibodies capable of detecting Mena^{INV} protein present in FNA biopsies (14). Thus, the quantification of Mena isoform expression at the protein level was not performed in this study.

Similar to our previous study on samples from 40 patients (14), the new cohort of 60 patients showed a strong positive correlation between Mena^{INV} score and TMEM ($r = 0.62$, $P = 10^{-6}$) and a weak negative correlation between Mena11a score and TMEM ($r = -0.17$, $P = 0.19$), as did the combined cohort of 100 patients (14) (Fig. 1B). These data support the previous finding that Mena^{INV} may promote intravasation of human IDCs of the breast, whereas Mena11a may suppress intravasation.

Mena^{INV} and TMEM number correlate with each other regardless of clinical subtype and tumor grade

Because breast cancer is a heterogeneous disease, we investigated whether the Mena^{INV}-TMEM correlation is similar across the most common clinical subtypes and grades according to hormone receptor and *HER2* expression status. We observed a very strong correlation between TMEM and Mena^{INV} scores in the ERPR^{+}/HER2^{-} [estrogen receptor– and pro-gesterone receptor–positive, EGF receptor 2 (also known as ErbB2 or neu)–negative] subtype (Fig. 1C). Triple-negative (TN) cases showed a strong correlation, whereas the Mena^{INV}-TMEM correlation in HER2^{+} cases was moderate. Using a regression model fit to the rank-transformed data, we observed that the differences in slopes between the tumor types were not statistically significant. Thus, although there were differences in the Spearman correlation coefficient among the clinical subtypes, this difference was not statistically significant and suggests that relative Mena^{INV} transcript expression correlates with intravasation-rich microenvironments in the most common clinical subtypes of breast cancer. We observed only weak correlation in 14 cases that were ER^{+}/HER2^{-} but lacked PR expression (table S2). This weak correlation may be due to an inadequate statistical power. However, both ER and PR signaling are very complex and involve various paracrine components. There is evidence that signaling through PR is important not only for cell proliferation and branching of breast ducts but also for extra-cellular matrix remodeling and angiogenesis (26). Thus, it is plausible that a lack of PR signaling affects either TMEM

formation or Mena^{INV} transcript expression independently, resulting in observed lack of correlation.

In analyzing whether the Mena^{INV}-TMEM correlation was affected by tumor grade, we found that the correlation was strong in poorly and moderately differentiated tumors, and very strong in well-differentiated tumors (Fig. 2A). The regression model fit to the rank-transformed data again showed that the differences in slopes between tumor grades were not statistically significant; therefore, Mena^{INV}-TMEM correlation was not affected by tumor grade. Poorly differentiated IDCs grew in sheets transversed by blood vessels; moderately differentiated IDC grew in a combination of glands and sheets; and well-differentiated IDC typically grew in glands and cords surrounded by stroma containing blood vessels (Fig. 2B). Because of the proliferative pattern, cancer cells in well-differentiated IDC were rarely found in direct contact with perivascular macrophages, thus explaining the low TMEM score (Fig. 2A). These “TMEM-low” micro-environments in well-differentiated cases also showed low Mena^{INV} scores, thus strongly correlating.

The data thus far indicate that relative Mena^{INV} transcript abundance in FNA samples positively correlates with the presence of TMEM-rich microenvironments in common clinical subtypes of IDCs and across all breast tumor grades.

Mena^{INV} and TMEM scores independently correlate with clinical and pathological parameters

Because high TMEM score correlates with metastatic outcome, and Mena^{INV} score correlates with TMEM score, we assessed whether Mena^{INV} and TMEM scores in our cohort independently correlate with known clinical and pathological parameters associated with prognosis. We quantified TMEM score and relative Mena^{INV} expression in tumors of different grade, size, lymph node (LN) status, as well as hormone receptor and HER2 status (table S3). We found significant differences in TMEM score and relative Mena^{INV} expression, independently, only between well-differentiated and poorly differentiated tumors (Fig. 2C). This is likely due to the differential cell proliferation pattern among the grades, as discussed above. There was no significant difference in either TMEM score or relative Mena isoform expression among tumors of different size, LN status, or hormone receptor and *HER2* expression. When we examined LN status within each clinical subtype, we observed a somewhat positive correlation of LN positivity with TMEM score and relative Mena^{INV} expression only in ERPR^{+}/HER2^{-} tumors, but this did not reach statistical significance (fig. S2). These data indicate that TMEM and Mena^{INV} scores measure aspects of tumor biology not addressed by the current clinical and pathological parameters other than tumor grade.

E-cadherin expression in tumors differs among samples according to Mena^{INV} and TMEM scores

Tumor grade reflects mitotic count, nuclear features, and cancer cell growth pattern. Because architectural tumor growth pattern was associated with TMEM formation (Fig. 2B), we investigated whether other aspects of tumor architecture would differ among cases with low and high TMEM and Mena^{INV} scores. Cell cohesion is one aspect of tumor biology that

is not measured by current clinical and pathological parameters. The ability of tumor cells to migrate toward blood vessels, assemble TMEMs, and intravasate is believed to require the epithelial-to-mesenchymal transition (EMT) and the disruption of epithelial junctions. We previously found that discohesion of epithelial cell-cell contacts in mouse mammary tumors is associated with Mena^{INV} score, which is associated with increased TMEM score (14). We predicted that this was also true in samples of human breast cancer. We observed significantly more cells with strong staining of cell-cell junction protein E-cadherin in cases with low TMEM and Mena^{INV} scores than in the cases with high TMEM and Mena^{INV} scores (Fig. 3A). Conversely, there were more cells with low E-cadherin abundance in cases with high TMEM and Mena^{INV} scores (Fig. 3B), indicating a correlation between discohesion and the Mena^{INV}/TMEM phenotype, as predicted.

Mena^{INV} isoform expression is associated with TEM-competent breast carcinoma cells

On the basis of the above results and previous work indicating that Mena^{INV} potentiates breast cancer cell intravasation, dissemination, and lung metastases in vivo (4), we hypothesized in primary tumor cells from patients that Mena^{INV} expression is linked to TEM. Because human breast cancers with a high Mena^{INV}/high TMEM score have less E-cadherin abundance and are less cohesive, we anticipated that a population of discohesive, breast carcinoma cells with high Mena^{INV} scores could be obtained from patients by FNA biopsy to test this hypothesis. In addition, our previous study showed that the Mena isoform expression pattern in FNA samples reflects the cohesion or discohesion state of the cells in the tumor. In particular, smearing patterns of cells obtained by FNA from PyMT mice bearing late-stage tumors are significantly more discohesive (less aggregated) and expressed significantly more Mena^{INV} than those from cells from early-stage tumors (14). Therefore, we collected cancer cells by FNA from 32 patients with IDC of the breast of various clinical subtypes (14) and evaluated them in an in vitro subluminal-to-luminal TEM [intravasation-directed TEM (iTEM)] assay. The luminal side of the endothelium is defined as the cell surface facing the bottom well of the iTEM chamber containing complete medium and colony-stimulating factor-1 (CSF-1) (fig. S1A). Clinical and pathological parameters from the 32 cases used in the iTEM assay are summarized in tables S4 and S5.

Sixteen cases were examined in assays using immortalized human microvascular endothelial cell line (HMEC-1) cells to form the endothelium (fig. S3A), and 16 cases were examined using an endothelium derived from primary human umbilical vein endothelial cells (HUVECs) (Fig. 4, A to D). Similar results were obtained with these two endothelial cell populations. Before performing the iTEM assay, FNA samples were analyzed for the presence of cancer cells and macrophages by IHC for keratin and CD68 abundance, respectively (fig. S3B). In each sample, about 97% of the cells were keratin-positive cancer cells. According to intravital imaging studies, only about 2.5% of breast cancer cells are migratory (15), and of these, only about 40% have an embryonic expression pattern, including high Mena^{INV} expression (27). Thus, we expected only about 1% of cells from the total aspirate to be iTEM-competent. The addition of macrophages significantly increased iTEM activity of tumor cells (Fig. 4A); therefore, unless otherwise noted, experiments were performed in the presence of macrophages. This macrophage requirement for iTEM in vitro closely resembles cancer cell intravasation in vivo as observed by intravital imaging of

mouse mammary tumors (5). In 5 of 32 cases, no cells crossed the endothelial barrier (fig. S3A). In the remaining 27 cases that showed iTEM activity, cells that crossed the endothelial layer exhibited a 3- to 15-fold greater Mena^{INV} abundance than that in the original population of cells loaded (fig. S3A and Fig. 4B). In cells that crossed the endothelium, there was no significant difference in relative Mena^{INV} expression between clinical subtypes (Fig. 4C).

The ability of cancer cells to cross the HUVEC endothelium was studied at single-cell resolution by imaging. We observed that cancer cells from all subtypes dissociated endothelial cell-cell junctions at the sites of transmigration and that they transmigrated in close proximity to macrophages (Fig. 4D). These data indicate that macrophage-mediated iTEM activity is present in all three clinical subtypes.

Similar results were obtained using FNA-collected cancer cells from xenografts derived from two human TN breast cancer tumor tissues (Fig. 4, E and F). The tumor grafts were described previously (9). The iTEM-competent cells from both human xenografts expressed 60- to 70-fold more Mena^{INV} abundance than did the original cell population (Fig. 4E). These data indicate that Mena^{INV} is associated with iTEM in human IDC tissue transplants in mice and primary human breast IDCs irrespective of clinical subtype.

Mena^{INV} promotes iTEM of tumor cells

To assess whether the expression of Mena^{INV} has a causal or promotional role in iTEM, or is instead an acquired trait in tumor cells after iTEM, Mena^{INV} was selectively knocked down in the TN human breast cancer cell line MDA-MB-231. The expression of the transcripts encoding Mena11a, Mena^{INV}, or total Mena (cumulative detection of all isoforms) was quantified using qPCR after transfection with control or one of three Mena^{INV}-targeted siRNAs (small interfering RNAs) (Fig. 5A). We observed a significant decrease in iTEM activity in cells depleted of Mena^{INV} compared to control cells (Fig. 5B). In addition, the overexpression of green fluorescent protein (GFP)–tagged Mena^{INV} in MDA-MB-231 cells caused a significant increase in macrophage-induced iTEM compared to cells expressing GFP alone, and this increased iTEM of GFP-Mena^{INV}–overexpressing cells was suppressed to baseline by Mena^{INV} knockdown (Fig. 5C). Together, these data indicate that Mena^{INV} is required for tumor cell iTEM.

iTEM-competent cells from TN and HER2$^+$ IDCs have increased abundance of the CSF-1 receptor

Increased CSF-1R (CSF-1 receptor) abundance in human TN mammary tumor cell lines results in a decreased reliance on macrophages for invasion and migration due to autocrine signaling (28, 29). The transmigration of cancer cells from ERPR$^+$/HER2$^-$ cases was associated with a higher number of macrophages located in close proximity to tumor cells compared with those in TN and HER2$^+$ cases (Fig. 6A). Because clinical subtypes exhibit differences in the extent of tumor-associated macrophages during transmigration, and because CSF-1 is present in the bottom well of the iTEM assay, we investigated whether CSF-1R abundance in tumor cells differed among iTEM-competent cells from ERPR$^+$/HER2$^-$, TN, and ERPR$^-$/HER2$^+$ cancers. An examination of CSF-1R expression in iTEM-

competent cells from these clinical subtypes as well as from TN tissue transplants revealed little or no enrichment of CSF-1R expression in iTEM-competent cells from $ERPR^+/HER2^-$ tumors; however, iTEM-competent cells from TN and $ERPR^-/HER2^+$ tumors had substantially more CSF-1R expression compared to the total FNA load (Fig. 6, B and C). These results suggest that CSF-1R–dependent autocrine signaling in TN and $ERPR^-/HER2^+$, but not in $ERPR^+/HER2^-$, accounts for the decreased numbers of macrophages associated with TN and $ERPR^-/HER2^+$ tumor cells during iTEM.

To investigate which signaling loops operate in IDC cells obtained from patients, we used an antibody specific for human CSF-1R (MAB3291) to block autocrine signaling specifically associated with the human CSF-1R present on human cancer cells, and an antibody specific for mouse CSF-1R (AFS98) to block paracrine signaling specifically associated with the mouse CSF-1R present on BAC1.2 mouse macrophages. Only inhibition of the mouse CSF-1R significantly reduced iTEM of $ERPR^+/HER2^-$ cells, indicating that only the paracrine signaling mediates the transmigration activity of this breast cancer subtype. However, blockade of both the mouse and human CSF-1Rs significantly inhibited iTEM in TN and $ERPR^-/HER2^+$ cancer cells (Fig. 6D). Similar results were obtained by blocking the mouse or human CSF-1R in the TN human tissue transplants HT17 and HT39 (Fig. 6, E and F). In addition, blocking both mouse and human CSF-1R brought iTEM to baseline levels (Fig. 6F). These data indicated that TN and $ERPR^-/HER2^+$ cells use both paracrine and autocrine signaling for transmigration activity.

Primary human macrophages enhance the iTEM activity of primary human breast cancer cells

Previous work demonstrated that several macrophage cell lines such as murine BAC1.2F5, immortalized bone marrow–derived macrophage cell line (iBMM), and RQW264.7 support iTEM in vitro (30). We wanted to assess whether primary human macrophages affected the iTEM of cancer cells in a similar fashion as do macrophage cell lines. Indeed, primary human macrophages substantially increased the iTEM activity of cells from human primary TN breast cancer xenografts HT17 and HT39 (Fig. 7A). Additionally, iTEM-competent cells showed greater $Mena^{INV}$ expression (Fig. 7B) and greater CSF-1R expression (Fig. 7C) than the load. Furthermore, imaging at the single-cell resolution revealed transmigration of cancer cells in close proximity to macrophages as well as the dissociation of endothelial cell-cell junctions at the sites of transmigration (Fig. 7D). Thus, primary human macrophages affect iTEM of TN primary human breast cancer cells in the same manner as do macrophage cell lines.

DISCUSSION

Here, we tested the hypothesis that relative $Mena^{INV}$ isoform expression is linked to TMEM number and the iTEM of tumor cells in human breast cancer by measuring the iTEM activity of primary tumor cells from patients. To our knowledge, this is the first study to use primary tumor cells obtained from patient breast cancers by FNA for functional iTEM assays in vitro.

We found that the abundance of Mena^{INV}, but not Mena11a, correlated positively with the number of TMEM intravasation sites in a cohort of 100 breast IDCs. Although human breast cancer is a heterogeneous disease consisting of several distinct subtypes with substantially different responses to therapy and clinical outcomes, we did not find statistically significant differences in the correlation between relative Mena^{INV} abundance and TMEM counts among the three clinically distinct subtypes: ERPR^{+}/ HER2^{-}, TN, and HER2^{+}. This suggests that a Mena^{INV}-TMEM–mediated mechanism of intravasation is present in all three disease subtypes; however, these conclusions need to be confirmed on a larger breast cancer cohort (31).

In accordance with previous work, we found that, due to their growth pattern, low-grade tumors have significantly lower TMEM score than poorly differentiated tumors (14, 22). Unlike previous studies, most likely because of our larger cohort size, we found significantly higher relative Mena^{INV} abundance in poorly differentiated cases compared to well-differentiated cases. We did not find any correlations between relative Mena isoform expression or TMEM score and LN status, tumor size, ER, PR, or HER2 status, which is also in accordance with previous studies (22, 23).

High abundance of Mena^{INV} and high TMEM counts were both correlated with reduced E-cadherin staining in human tumors. A recent study using a human mammary epithelial cell line that had been modified to mesenchymal phenotype by forced expression of the EMT transcription factor Twist (HMLE/pBP-Twist) supports a role for Mena11a in conferring epithelial, cohesive, noninvasive cell behavior (32). In particular, expression of splicing factor ESRP1 (epithelial-specific RNA binding protein 1) in HMLE/ pBP-Twist cells induced Mena11a expression and promoted epithelial-like reorganization of peripheral actin, cell-cell junctions, and suppressed mesenchymal-like migration (32). Because overexpression of Mena^{INV} in rodent mammary tumors decreases cell cohesion, E-cadherin, and β-catenin expression (14), we anticipated that human breast cancer cases with high Mena^{INV}-TMEM scores would have less E-cadherin abundance than those with low Mena^{INV}-TMEM scores. Moreover, we documented previously that alternative splicing, a process that regulates Mena isoform expression, can induce EMT-like phenotypic changes, such as actin cytoskeleton remodeling, cell-cell junction formation, and cell migration (32). Similarly to the Mena^{INV} and TMEM scores, E-cadherin abundance did not correlate with clinically used prognostic parameters such as tumor size, grade, LN status, and hormonal or *HER2* expression (33). However, some studies indicate that reduced E-cadherin abundance in IDCs is associated with high histologic grade, loss of *ER* expression, and shorter disease-free survival (34). This suggests that high Mena^{INV} expression score, low E-cadherin abundance, and high TMEM score—associated with worse clinical outcome—reflect aspects of tumor biology that are not captured in currently used clinical and pathological parameters.

Using an iTEM assay with human primary tumor cells obtained by FNA, we demonstrated that the iTEM-competent subset of human IDC cells of all clinical subtypes has increased expression of Mena^{INV} but not Mena11a (Fig. 8). This result is also consistent with a recent study showing that loss of Mena11a relative to total Mena abundance in breast tumor tissue was a prognostic marker for poor outcome in two large breast cancer cohorts (35). These

data indicate that the Mena^{INV} isoform is associated with iTEM in primary human IDCs of the breast irrespective of clinical subtype. Our data are in accordance with the results obtained with MTLn3 cells overexpressing various Mena isoforms (6). In that study, only MTLn3 cells overexpressing Mena^{INV} in the presence of macrophages showed significant iTEM (6). Here, using three different Mena^{INV}-targeted siRNAs or the overexpression of GFP-Mena^{INV}, we demonstrated that Mena^{INV} promotes iTEM in TN human breast cancer cell line MDA-MB-231. Thus, Mena^{INV} not only is associated with iTEM but also functionally promotes iTEM activity in tumor cells.

It is now well recognized that tumor-associated macrophages contribute to tumor progression and metastasis, as well as to the response to anti-cancer therapies (30, 36, 37). Macrophages facilitate cancer cell intravasation in at least two ways. First, they comigrate with cancer cells using a chemotactic paracrine signaling loop consisting of macrophage-secreted EGF [which activates EGFR (EGF receptor) on cancer cells] and cancer cell–secreted CSF-1 (which activates CSF-1R on macrophage). This paracrine loop results in migratory cell streams, which efficiently move toward perivascular macrophages (8, 10, 38). Second, the direct physical contact between perivascular macrophages and cancer cells induces RhoA activity and enhances the formation of invadopodia, actin-rich matrix-degrading protrusions that are required for iTEM (7, 8, 39). Both streaming and iTEM are macrophage-dependent tumor cell behaviors that are amplified by Mena^{INV} expression (6, 16). The claudin-low subtype of TN human breast cancer cells also communicates through an autocrine CSF-1–CSF-1R loop (28, 29). Human breast cancer cells express CSF-1R under the control of TGFβ (transforming growth factor–β) signaling, demonstrating a role of the tumor microenvironment in the induction of CSF-1R expression in human cancer cells (28, 29). TGFβ also induces CSF-1R expression in cultured cells, and the presence of estradiol in ER$^+$ cells suppresses the expression of TGFβ-induced genes, possibly through ER-meditated degradation of the TGFβ effectors, SMADs (40). We demonstrated here that iTEM-competent TN and HER2$^+$ cells express more CSF-1R than iTEM-competent ER$^+$/HER2 cells. We also demonstrated that breast cancer cells from ER$^+$/HER2$^-$ disease primarily use a paracrine loop, whereas cancer cells from TN and HER2$^+$ disease use a tumor cell autocrine loop involving CSF-1 in addition to the paracrine loop for iTEM (Fig. 8). This may be advantageous for their ability to invade and intravasate. Thus, the higher likelihood of developing distant recurrence and worse clinical outcome in TN and HER2$^+$ disease (41) may be in part due to autocrine signaling involving CSF-1R expression on cancer cells. Indeed, human breast cancers that coexpress CSF-1 and its receptor have worse outcome, and high expression of CSF-1 promotes metastatic progression in mouse cancer models (42, 43). Studies to thoroughly understand how CSF-1R, macrophages, and Mena^{INV} facilitate iTEM of human IDC cells are under way.

Overall, in addition to the potential for future clinical applications in prognosis and treatment of cancer, this study illustrates the value of using primary tumor cells from patients with different clinical subtypes to investigate the underlying biology behind tumor cell dissemination.

MATERIALS AND METHODS

Human tissue selection and FNA biopsy procedure

Lumpectomy and mastectomy specimens received at the Albert Einstein College of Medicine/Montefiore Medical Center, Moses and Weiler Divisions for pathological examination were used for FNA-based tissue collection under institutional review board approval. Four to five FNA aspiration biopsies per tumor were performed on grossly visible lesions using 25-gauge needles. The adequacy of the sample was assessed by the standard Diff-Quick protocol (44). Only samples composed of at least 90% malignant epithelial cells, as determined by standard pathologic characteristics (44), were used in the study. ER, PR, and HER2 receptor staining and scoring were done in accordance with United States and Canadian Academy of Pathology/American Society of Clinical Oncology (USCAP/ ASCO) guidelines (45, 46).

Intravasation TEM (iTEM)

The iTEM assay was performed as described previously (6) and briefly described here with modifications. The Transwell was prepared so that tumor cell TEM was in the intravasation direction [from subluminal side to luminal side of the endothelium (fig. S1A)]. We define this as the iTEM assay. To prepare the endothelial monolayer, the underside of each Transwell was coated with 50 μl of Matrigel (2.5 μg/ml; Invitrogen). About 100,000 HUVEC cells were plated on the Matrigel-coated underside of the Transwells. For HMEC-1 experiments, 200,000 human microvascular endothelial cells (HMEC-1) were plated. Transwells were then flipped onto a 24-well plate containing 200 μl of α-MEM (minimum essential medium) supplemented with 10% fetal bovine serum (FBS) + 3000 U of CSF-1 and incubated until the endothelium formed impermeable monolayers. Permeability of both monolayers was tested as described previously by diffusion of 70 kD of Texas Red dextran (fig. S1, C and D) (Molecular Devices SpectraMax M5 plate reader) and by electrical resistance (World Precision Instruments) (fig. S1, E and F) (39), which demonstrated that the monolayer was impermeable at 48 hours after plating of the HUVECs and HMECs; therefore, Transwells were used at this time point. HUVEC cells generated less permeable monolayers than HMECs; therefore, after the initial experiments, HUVECs were used exclusively. Once impermeable by these criteria, the Transwell assay was used for iTEM studies. All the assays were run in the presence of BAC1.2F5 murine macrophage cell line because it was demonstrated using cancer cell lines that iTEM of tumor cells is efficient only in the presence of macrophages (Fig. 4A) (6). Although it was shown previously that several other types of macrophages including immortalized bone marrow–derived macrophage cell line (iBMM) and the RQW264.7 support iTEM in vitro (39), we chose to do most of the work with BAC1.2F5 cell line, because it generated the most consistent and robust iTEM (39).

We confirmed major findings using primary human macrophages. Peripheral blood mononuclear cells (PBMCs) from anonymous donors were isolated from the Leuko Pak obtained from blood bank. To purify PBMCs, we used density gradient centrifugation, followed by clearance of the remaining red blood cells using hypotonic lysis. The PBMCs were then differentiated into macrophages by adherence in the presence of recombinant human CSF-1 and used a week after isolation.

Macrophages and FNA-obtained tumor cells were labeled with cell tracker dyes. Then, 15,000 macrophages and 37,500 tumor cells were added to the upper chamber in 200 μl of Dulbecco's modified Eagle's medium (DMEM)/F12 supplemented with 0.5% FBS. After 18 hours of transmigration, the medium was removed from the top of the Transwell, and the migrated cells were scraped from the bottom of the plate and immediately subjected to qRT-PCR analysis.

For ZO-1 immunostaining, the Transwells were fixed in 4% para-formaldehyde, permeabilized with 1% Triton X-100, and stained with an anti–ZO-1 (Invitrogen). Transwells were imaged using a Leica SP5 confocal microscope using a 60× 1.4 numerical aperture objective and processed using ImageJ [National Institutes of Health (NIH)] and IMARIS programs. Quantitation was performed by counting the number of macrophages and tumor cells that had crossed the endothelium within the same field of view (60×, 10 random fields) and represented it as a ratio.

Human tissue transplants

The TN human tissue transplants HT17 and HT39 were previously described (9). Briefly, the tumor originated from human patient samples and have since only been propagated in SCID (severe combined immuno-deficient) mice. Tumors were harvested once they reached 1- to 1.2-cm diameter. Cells were obtained by FNA from human tumors grown in mice, and experiments were carried out in the same manner as was done with direct patient samples. All procedures were conducted in accordance with the NIH regulations and approved by the Albert Einstein College of Medicine animal use committee.

CSF-1R blocking experiments

Inhibition of the mouse or human CSF-1R was done using the following species-specific blocking antibodies: monoclonal rat anti-mouse CSF-1R (AFS98) or monoclonal mouse anti-human CSF-1R (MAB3291; R&D Systems) (47) at final concentrations of 50 μg/ml. Transwells were prepared as described above, and blocking antibody or control immunoglobulin G (IgG) was added to the top well containing tumor cells and macrophages.

Quantitative real-time polymerase chain reaction

qRT-PCR for Mena splice variants was performed as described previously (15). Briefly, the data analysis was conducted using the $\Delta\Delta C_t$ method, in which all *MENA* C_t values in the carcinoma samples were first normalized to *GAPDH*. A subsequently generated Mena score indicated the relative amount of Mena isoforms in the IDCs compared to the average fold change of Mena isoforms detected in five fibroadenomas, using the $\Delta\Delta C_t$ values for each sample. The data are referred to as either the Mena score or the relative Mena expression. qRT-PCR for Mena splice variants in the iTEM assay was also conducted using the $\Delta\Delta C_t$ method, in which all *MENA* C_t values in TEM-competent cells were first normalized to *GAPDH*. Subsequently, relative isoform levels were estimated by comparing the normalized C_t values of Mena isoforms in the cells that crossed the endothelium to the *GAPDH*-normalized C_t values of Mena isoforms present in the starting sample. qRT-PCR analyses were performed with a SYBR Green kit (Qiagen) and analyzed with ABI 7300 sequence

detector and associated software (Applied Biosystems). Primers detecting transcripts encoding Mena^{INV} and Mena11a are described in table S1.

Tissue selection for TMEM staining and scoring

At the time of routine microscopic examination of the lesions on which FNA biopsies had been performed, an appropriate area containing invasive cancer suitable for TMEM analysis was identified by low-power scanning using the following criteria: high density of tumor, adequacy of tumor, lack of necrosis or inflammation, and lack of artifacts such as retraction or folds. TMEM stain is a triple immunostain for predicting metastatic risk in which three antibodies are applied sequentially and developed separately with different chromogens on a Bond Max autostainer (Leica Biosystems). The pan-Mena mouse monoclonal antibody (A351F7D9) was produced in the Gertler laboratory and is not commercially available. The assessment of TMEM scores was performed with Adobe Photoshop on 10 contiguous 400× digital images of the most representative areas of the tumor. The total TMEM for each image was tabulated, and the scores from all 10 images were summed to give a final TMEM density for each patient sample, expressed as the number of TMEM per total magnification (ten 400× fields) (22). Twenty-five randomly chosen cases were each independently scored by two pathologists. Because the correlation between the scores was excellent, with a correlation coefficient $r = 0.97$, the remaining 75 cases were scored by one pathologist.

Relationship of FNA sample to TMEM

FNA primarily collects loose tumor cells, with very few macrophages and no endothelial cells, and incurs minimal tissue damage (48). After the FNA procedure, the entire tumor was fixed in formalin and embedded in paraffin and sent for pathological examination. A representative block of FFPE tumor tissue was selected and triple immunostained for TMEMs. Therefore, each tumor was sampled by FNA for Mena isoform expression analysis and by FFPE for TMEM scoring (14).

IHC and scoring of E-cadherin

IHC for E-cadherin was done using commercially available monoclonal antibody against E-cadherin (Dako; 1:25 dilution). Antigen retrieval was performed in a steamer at 90°C for 30 min in Target Retrieval Solution (pH 6.0). The slides were incubated with the primary antibody for 30 min at room temperature and for 30 min with a secondary antibody. E-cadherin was visualized using horseradish peroxidase (HRP)–conjugated mouse-specific antibody (EnVision System, Dako) and DAB (diaminobenzidine) on an automated immunostainer (Autostainer, Dako) according to the manufacturer's instructions. The slides were counterstained with hematoxylin using standard techniques.

Similarly to TMEM scoring, 10 digital images were acquired at 400× total magnification for each tumor and scored by two pathologists as follows: 3, strong complete membranous staining; 2, moderate complete membranous staining; 1, weak incomplete membranous staining; 0, no staining. The cells within each scoring category were labeled with different Photoshop tools. Data were summed from all 10 images to give a final mean number (and percentage, with error) of cells per tumor with each score. Ten cases of low Mena^{INV}–low TMEM score (Mena$^{INV} < 1$, and TMEM < 10) and 10 cases of high Mena^{INV}–high TMEM

score ($Mena^{INV}$ > 5, and TMEM > 50) were analyzed for E-cadherin staining intensity. The cutoff levels for high and low scores were established on the basis of the scores above the top 85th and below the low 25th percentile

IHC and scoring of keratin and CD68-positive cells

Keratin staining was done on FNA samples prepared as cytospins. The staining was performed in an automatic slide stainer (Dako Autostainer Plus). The primary mouse monoclonal antibody AE13 (catalog no. M3515, Dako; 1:200) and mouse monoclonal antibody CD68 (catalog no. M0814, Dako; 1:2000) were applied for 30 min at room temperature, followed by 30 min in HRP-conjugated anti-mouse secondary antibody (DakoCytomation EnVision+ System, catalog no. K400111). Slides were incubated with DAB Substrate kit (Dako) for 5 min, counterstained with Surgipath Hematoxylin (Fisher HealthCare), dehydrated through graded alcohols, cleared in xylene, and cover-slipped with CytoSeal 60 (Richard-Allen Scientific). The whole cytospin area (314 mm^2) was scored for AE1: AE3 and CD68-positive cells; data are presented as a percentage of positive cells.

Small interfering RNA

Isoform-specific knockdown of $Mena^{INV}$ in MDA-MB-231 cells was achieved using siRNA. Transfections were performed by resuspending 8×10^5 cells in a 100 μl of Lonza kit V transfection solution with 2 μM siRNA for 96 hours. $Mena^{INV}$ siRNA was purchased from Ambion (Custom Select siRNA). Knockdown efficiency was measured by qPCR.

Statistical analysis

The strength of the association between *MENA* isoform expression and TMEM density was calculated using rank-order correlation and represented by Spearman's correlation coefficient. Wilcoxon-Mann-Whitney rank sum test was used to assess the differences between TMEM density and relative *MENA* expression in terms of their association with tumor grade, LN status, tumor size, ER, PR, and HER2/Neu status. A regression model fit was used to rank-transformed data and assess the differences in slopes among tumor types. Given that six comparisons were done for human samples, the *P* value for determining statistical significance was set at 0.008 by applying the Bonferroni correction to the standard assumption that $P < 0.05$ is statistically significant. Statistical significances in E-cadherin abundance as well as the difference in expression of genes encoding for Mena isoforms and CSF-1R in intravasation-competent cells between clinical subtypes were determined using unpaired, two-tailed Student's *t* tests assuming equal variances and an α level of 0.05. Differences were considered significant if $P < 0.05$. Actual *P* values are listed on the graphs or in the legends of each figure.

Supplementary Material

Refer to Web version on PubMed Central for supplementary material.

Acknowledgments

We would like to acknowledge M. Kim's help in assessing the differences in slopes among tumor types and Y. Wang and A. Patsialou for assistance with human tissue transplants.

Funding: This work was supported by grants from the NIH (CA170507-01 to J.P., X.C., J.S.C., E.A., M.H.O., and S.G.; CA100324 to S.G., T.E.R., and A.B.), the Breast Cancer Alliance (S.G.), the Department of Defense Breast Cancer Research Program (W81XWH-14-1-0286 to J.P.), and the Albert Einstein College of Medicine Integrated Imaging Program (J.G.J.).

REFERENCES AND NOTES

1. Chaffer CL, Weinberg RA. A perspective on cancer cell metastasis. Science. 2011; 331:1559–1564. [PubMed: 21436443]
2. Tevaarwerk AJ, Gray RJ, Schneider BP, Smith ML, Wagner LI, Fetting JH, Davidson N, Goldstein LJ, Miller KD, Sparano JA. Survival in patients with metastatic recurrent breast cancer after adjuvant chemotherapy: Little evidence of improvement over the past 30 years. Cancer. 2013; 119:1140–1148. [PubMed: 23065954]
3. Wang W, Wyckoff JB, Frohlich VC, Oleynikov Y, Huttelmaier S, Zavadil J, Cermak L, Bottinger EP, Singer RH, White JG, Segall JE, Condeelis JS. Single cell behavior in metastatic primary mammary tumors correlated with gene expression patterns revealed by molecular profiling. Cancer Res. 2002; 62:6278–6288. [PubMed: 12414658]
4. Wyckoff J, Gligorijevic B, Entenberg D, Segall J, Condeelis J. High-resolution multiphoton imaging of tumors in vivo. Cold Spring Harb Protoc. 2011; 2011:1167–1184. [PubMed: 21969629]
5. Wyckoff JB, Wang Y, Lin EY, Li JF, Goswami S, Stanley ER, Segall JE, Pollard JW, Condeelis J. Direct visualization of macrophage-assisted tumor cell intravasation in mammary tumors. Cancer Res. 2007; 67:2649–2656. [PubMed: 17363585]
6. Entenberg D, Wyckoff J, Gligorijevic B, Roussos ET, Verkhusha VV, Pollard JW, Condeelis J. Setup and use of a two-laser multiphoton microscope for multichannel intravital fluorescence imaging. Nat Protoc. 2011; 6:1500–1520. [PubMed: 21959234]
7. Wyckoff J, Wang W, Lin EY, Wang Y, Pixley F, Stanley ER, Graf T, Pollard JW, Segall J, Condeelis J. A paracrine loop between tumor cells and macrophages is required for tumor cell migration in mammary tumors. Cancer Res. 2004; 64:7022–7029. [PubMed: 15466195]
8. Goswami S, Sahai E, Wyckoff JB, Cammer M, Cox D, Pixley FJ, Stanley ER, Segall JE, Condeelis JS. Macrophages promote the invasion of breast carcinoma cells via a colony-stimulating factor-1/epidermal growth factor paracrine loop. Cancer Res. 2005; 65:5278–5283. [PubMed: 15958574]
9. Patsialou A, Wang Y, Lin J, Whitney K, Goswami S, Kenny PA, Condeelis JS. Selective gene-expression profiling of migratory tumor cells in vivo predicts clinical outcome in breast cancer patients. Breast Cancer Res. 2012; 14:R139. [PubMed: 23113900]
10. Condeelis J, Singer RH, Segall JE. The great escape: When cancer cells hijack the genes for chemotaxis and motility. Annu Rev Cell Dev Biol. 2005; 21:695–718. [PubMed: 16212512]
11. Gertler F, Condeelis J. Metastasis: Tumor cells becoming MENAcing. Trends Cell Biol. 2011; 21:81–90. [PubMed: 21071226]
12. Bagorda A, Mihaylov VA, Parent CA. Chemotaxis: Moving forward and holding on to the past. Throm Haemost. 2006; 95:12–21.
13. Wang W, Mouneimne G, Sidani M, Wyckoff J, Chen X, Makris A, Goswami S, Bresnick AR, Condeelis JS. The activity status of cofilin is directly related to invasion, intravasation, and metastasis of mammary tumors. J Cell Biol. 2006; 173:395–404. [PubMed: 16651380]
14. Roussos ET, Goswami S, Balsamo M, Wang Y, Stobezki R, Adler E, Robinson BD, Jones JG, Gertler FB, Condeelis JS, Oktay MH. Mena invasive ($Mena^{INV}$) and Mena11a isoforms play distinct roles in breast cancer cell cohesion and association with TMEM. Clin Exp Metastasis. 2011; 28:515–527. [PubMed: 21484349]
15. Patsialou A, Bravo-Cordero JJ, Wang Y, Entenberg D, Liu H, Clarke M, Condeelis JS. Intravital multiphoton imaging reveals multicelluar streaming as a crucial component of in vivo cell migration in human breast tumors. Intravital. 2013; 2:e25294. [PubMed: 25013744]
16. Philippar U, Roussos ET, Oser M, Yamaguchi H, Kim HD, Giampieri S, Wang Y, Goswami S, Wyckoff JB, Lauffenburger DA, Sahai E, Condeelis JS, Gertler FB. A Mena invasion isoform potentiates EGF-induced carcinoma cell invasion and metastasis. Dev Cell. 2008; 15:813–828. [PubMed: 19081071]

17. Goswami S, Philippar U, Sun D, Patsialou A, Avraham J, Wang W, Di Modugno F, Nistico P, Gertler FB, Condeelis JS. Identification of invasion specific splice variants of the cytoskeletal protein Mena present in mammary tumor cells during invasion in vivo. Clin Exp Metastasis. 2009; 26:153–159. [PubMed: 18985426]

18. Mouneimne G, DesMarais V, Sidani M, Scemes E, Wang W, Song X, Eddy R, Condeelis J. Spatial and temporal control of cofilin activity is required for directional sensing during chemotaxis. Curr Biol. 2006; 16:2193–2205. [PubMed: 17113383]

19. Di Modugno F, Mottolese M, Di Benedetto A, Conidi A, Novelli F, Perracchio L, Venturo I, Botti C, Jager E, Santoni A, Natali PG, Nisticò P. The cytoskeleton regulatory protein hMena (ENAH) is overexpressed in human benign breast lesions with high risk of transformation and human epidermal growth factor receptor-2–positive/hormonal receptor–negative tumors. Clin Cancer Res. 2006; 12:1470–1478. [PubMed: 16533770]

20. Pino MS, Balsamo M, Di Modugno F, Mottolese M, Alessio M, Melucci E, Milella M, McConkey DJ, Philippar U, Gertler FB, Natali PG, Nisticò P. Human Mena^{+11a} isoform serves as a marker of epithelial phenotype and sensitivity to epidermal growth factor receptor inhibition in human pancreatic cancer cell lines. Clin Cancer Res. 2008; 14:4943–4950. [PubMed: 18676769]

21. Kühnel K, Jarchau T, Wolf E, Schlichting I, Walter U, Wittinghofer A, Strelkov SV. The VASP tetramerization domain is a right-handed coiled coil based on a 15-residue repeat. Proc Natl Acad Sci USA. 2004; 101:17027–17032. [PubMed: 15569942]

22. Robinson BD, Sica GL, Liu YF, Rohan TE, Gertler FB, Condeelis JS, Jones JG. Tumor microenvironment of metastasis in human breast carcinoma: A potential prognostic marker linked to hematogenous dissemination. Clin Cancer Res. 2009; 15:2433–2441. [PubMed: 19318480]

23. Rohan TE, Xue X, Lin HM, D'Alfonso TM, Ginter PS, Oktay MH, Robinson BD, Ginsberg M, Gertler FB, Glass AG, Sparano JA, Condeelis JS, Jones JG. Tumor microenvironment of metastasis and risk of distant metastasis of breast cancer. J Natl Cancer Inst. 2014; 106:dju136. [PubMed: 24895374]

24. Roussos ET, Wang Y, Wyckoff JB, Sellers RS, Wang W, Li J, Pollard JW, Gertler FB, Condeelis JS. Mena deficiency delays tumor progression and decreases metastasis in polyoma middle-T transgenic mouse mammary tumors. Breast Cancer Res. 2010; 12:R101. [PubMed: 21108830]

25. Roussos ET, Condeelis JS, Patsialou A. Chemotaxis in cancer. Nat Rev Cancer. 2011; 11:573–587. [PubMed: 21779009]

26. Brisken C. Progesterone signalling in breast cancer: A neglected hormone coming into the limelight. Nat Rev Cancer. 2013; 13:385–396. [PubMed: 23702927]

27. Liu H, Patel MR, Prescher JA, Patsialou A, Qian D, Lin J, Wen S, Chang YF, Bachmann MH, Shimono Y, Dalerba P, Adorno M, Lobo N, Bueno J, Dirbas FM, Goswami S, Somlo G, Condeelis J, Contag CH, Gambhir SS, Clarke MF. Cancer stem cells from human breast tumors are involved in spontaneous metastases in orthotopic mouse models. Proc Natl Acad Sci USA. 2010; 107:18115–18120. [PubMed: 20921380]

28. Patsialou A, Wyckoff J, Wang Y, Goswami S, Stanley ER, Condeelis JS. Invasion of human breast cancer cells in vivo requires both paracrine and autocrine loops involving the colony-stimulating factor-1 receptor. Cancer Res. 2009; 69:9498–9506. [PubMed: 19934330]

29. Patsialou A, Wang Y, Pignatelli J, Chen X, Entenberg D, Oktay M, Condeelis JS. Autocrine CSF1R signaling mediates switching between invasion and proliferation downstream of TGFβ in claudin-low breast tumor cells. Oncogene. 201410.1038/onc.2014.226

30. De Palma M, Lewis CE. Macrophage regulation of tumor responses to anticancer therapies. Cancer Cell. 2013; 23:277–286. [PubMed: 23518347]

31. Bertos NR, Park M. Breast cancer—One term, many entities? J Clin Invest. 2011; 121:3789–3796. [PubMed: 21965335]

32. Shapiro IM, Cheng AW, Flytzanis NC, Balsamo M, Condeelis JS, Oktay MH, Burge CB, Gertler FB. An EMT-driven alternative splicing program occurs in human breast cancer and modulates cellular phenotype. PLOS Genet. 2011; 7:e1002218. [PubMed: 21876675]

33. Singhai R, Patil VW, Jaiswal SR, Patil SD, Tayade MB, Patil AV. E-cadherin as a diagnostic biomarker in breast cancer. N Am J Med Sci. 2011; 3:227–233. [PubMed: 22558599]

34. Siitonen SM, Kononen JT, Helin HJ, Rantala IS, Holli KA, Isola JJ. Reduced E-cadherin expression is associated with invasiveness and unfavorable prognosis in breast cancer. Am J Clin Pathol. 1996; 105:394–402. [PubMed: 8604681]
35. Agarwal S, Gertler FB, Balsamo M, Condeelis JS, Camp RL, Xue X, Lin J, Rohan TE, Rimm DL. Quantitative assessment of invasive mena isoforms ($Mena^{calc}$) as an independent prognostic marker in breast cancer. Breast Cancer Res. 2012; 14:R124. [PubMed: 22971274]
36. Cortez-Retamozo V, Engblom C, Pittet MJ. Remote control of macrophage production by cancer. Oncoimmunology. 2013; 2:e24183. [PubMed: 23762799]
37. Fang H, Declerck YA. Targeting the tumor microenvironment: From understanding pathways to effective clinical trials. Cancer Res. 2013; 73:4965–4977. [PubMed: 23913938]
38. Dovas A, Gligorijevic B, Chen X, Entenberg D, Condeelis J, Cox D. Visualization of actin polymerization in invasive structures of macrophages and carcinoma cells using photoconvertible β-actin—Dendra2 fusion proteins. PLOS One. 2011; 6:e16485. [PubMed: 21339827]
39. Roh-Johnson M, Bravo-Cordero JJ, Patsialou A, Sharma VP, Guo P, Liu H, Hodgson L, Condeelis J. Macrophage contact induces RhoA GTPase signaling to trigger tumor cell intravasation. Oncogene. 2014; 33:4203–4212. [PubMed: 24056963]
40. Goto N, Hiyoshi H, Ito I, Tsuchiya M, Nakajima Y, Yanagisawa J. Estrogen and antiestrogens alter breast cancer invasiveness by modulating the transforming growth factor-β signaling pathway. Cancer Sci. 2011; 102:1501–1508. [PubMed: 21564419]
41. Rakha EA, Chan S. Metastatic triple-negative breast cancer. Clin Oncol (R Coll Radiol). 2011; 23:587–600. [PubMed: 21524569]
42. Kacinski BM. CSF-1 and its receptor in ovarian, endometrial and breast cancer. Ann Med. 1995; 27:79–85. [PubMed: 7742005]
43. Lin EY, Nguyen AV, Russell RG, Pollard JW. Colony-stimulating factor 1 promotes progression of mammary tumors to malignancy. J Exp Med. 2001; 193:727–740. [PubMed: 11257139]
44. Gupta PK, Baloch ZW. Intraoperative and on-site cytopathology consultation: Utilization, limitations, and value. Semin Diagn Pathol. 2002; 19:227–236. [PubMed: 12469790]
45. Hammond ME, Hayes DF, Dowsett M, Allred DC, Hagerty KL, Badve S, Fitzgibbons PL, Francis G, Goldstein NS, Hayes M, Hicks DG, Lester S, Love R, Mangu PB, McShane L, Miller K, Osborne CK, Paik S, Perlmutter J, Rhodes A, Sasano H, Schwartz JN, Sweep FC, Taube S, Torlakovic EE, Valenstein P, Viale G, Visscher D, Wheeler T, Williams RB, Wittliff JL, Wolff AC. American Society of Clinical Oncology; College of American Pathologists, American Society of Clinical Oncology/College of American Pathologists guideline recommendations for immunohistochemical testing of estrogen and progesterone receptors in breast cancer (unabridged version). Arch Pathol Lab Med. 2010; 134:e48–e72. [PubMed: 20586616]
46. Hammond ME, Hayes DF, Dowsett M, Allred DC, Hagerty KL, Badve S, Fitzgibbons PL, Francis G, Goldstein NS, Hayes M, Hicks DG, Lester S, Love R, Mangu PB, McShane L, Miller K, Osborne CK, Paik S, Perlmutter J, Rhodes A, Sasano H, Schwartz JN, Sweep FC, Taube S, Torlakovic EE, Valenstein P, Viale G, Visscher D, Wheeler T, Williams RB, Wittliff JL, Wolff AC. American Society of Clinical Oncology/College of American Pathologists guideline recommendations for immunohistochemical testing of estrogen and progesterone receptors in breast cancer. J Clin Oncol. 2010; 28:2784–2795. [PubMed: 20404251]
47. Pang H, Flinn R, Patsialou A, Wyckoff J, Roussos ET, Wu H, Pozzuto M, Goswami S, Condeelis JS, Bresnick AR, Segall JE, Backer JM. Differential enhancement of breast cancer cell motility and metastasis by helical and kinase domain mutations of class IA phosphoinositide 3-kinase. Cancer Res. 2009; 69:8868–8876. [PubMed: 19903845]
48. Symmans WF, Ayers M, Clark EA, Stec J, Hess KR, Sneige N, Buchholz TA, Krishnamurthy S, Ibrahim NK, Buzdar AU, Theriault RL, Rosales MF, Thomas ES, Gwyn KM, Green MC, Syed AR, Hortobagyi GN, Pusztai L. Total RNA yield and microarray gene expression profiles from fine-needle aspiration biopsy and core-needle biopsy samples of breast carcinoma. Cancer. 2003; 97:2960–2971. [PubMed: 12784330]

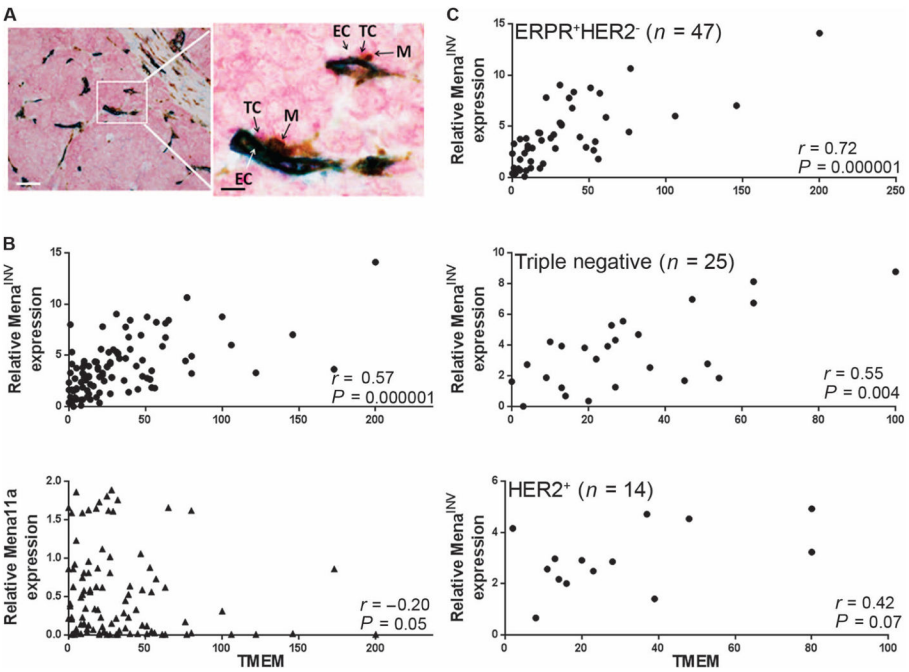

Fig. 1. Correlation of Mena isoform expression to TMEM score

(**A**) TMEM microanatomic cancer cell TEM sites visualized by IHC. TC, Mena-expressing tumor cells; EC, CD31-expressing vascular endothelial cells; M, CD68-expressing macrophages. Scale bars, 300 μm (left) and 50 μm (right). (**B** and **C**) Scatter plots of relative $Mena^{INV}$ transcript expression against TMEM score in the entire cohort of 100 IDCs (B) or by clinical subtype (C). Data were analyzed by rank-order correlation. The differences in slopes between subtypes were not statistically significant as shown by the regression model fit to the rank-transformed data. *n*, number of tumor cases.

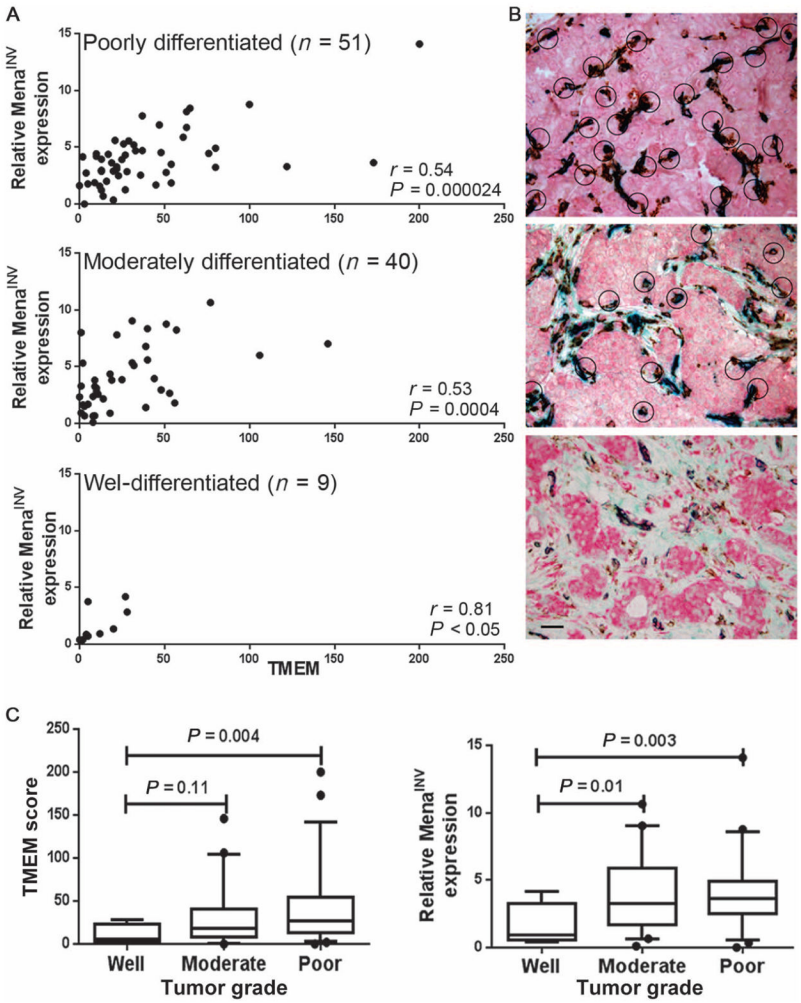

Fig. 2. Correlation of Mena^{INV}-TMEM scores in different grades of human IDCs

(**A**) Scatter plots of relative Mena^{INV} transcript expression against TMEM score in IDCs of different grades. Data were analyzed with Spearman's rank-order correlation. The differences in slopes between grades were not statistically significant as shown by the regression model fit to the rank-transformed data. (**B**) Representative microscopy of poorly differentiated (upper), moderately differentiated (lower), and well-differentiated (bottom) IDCs triple-stained for TMEM. TMEM sites are indicated by circles. Scale bar, 100 μm. (**C**) TMEM score (left panel) and relative Mena^{INV} transcript abundance (right panel) according to tumor grade. Median, 5th and 95th percentile for Mena^{INV} fold change, and TMEM score are presented for well-differentiated (n = 9), moderately differentiated (n = 40), and poorly differentiated (n = 51) tumors. Analyses were done using the Mann-Whitney U test at a statistical significance threshold of 0.008.

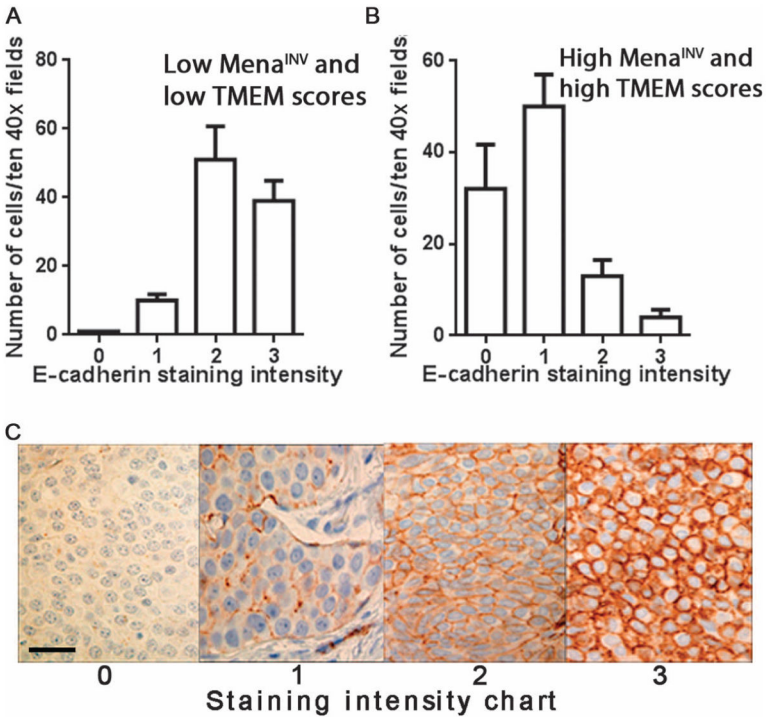

Fig. 3. Correlation of E-cadherin and TMEM and Mena^{INV} scores

(**A** and **B**) E-cadherin abundance in tumor tissues classified as either (A) low TMEM and low Mena^{INV} (scores <10 and <1, respectively) or high TMEM and high Mena^{INV} (scores >50 and >5, respectively). (**C**) Representative images showing staining scores of 0 (none) to 3 (strong). Data are means ± SEM from ten 40× fields scored from 10 cases in each group. $P < 0.001$, number of cells in the low TMEM-Mena^{INV} group that had moderate to strong E-cadherin staining (2 and 3) compared with that in the high TMEM-Mena^{INV} group. $P < 0.0001$, number of cells in the high TMEM-Mena^{INV} group that had none to weak E-cadherin staining (0 and 1) compared with that in the low TMEM-Mena^{INV} group. Data were analyzed with unpaired, two-tailed Student's *t* tests assuming equal variances and an α level of 0.05.

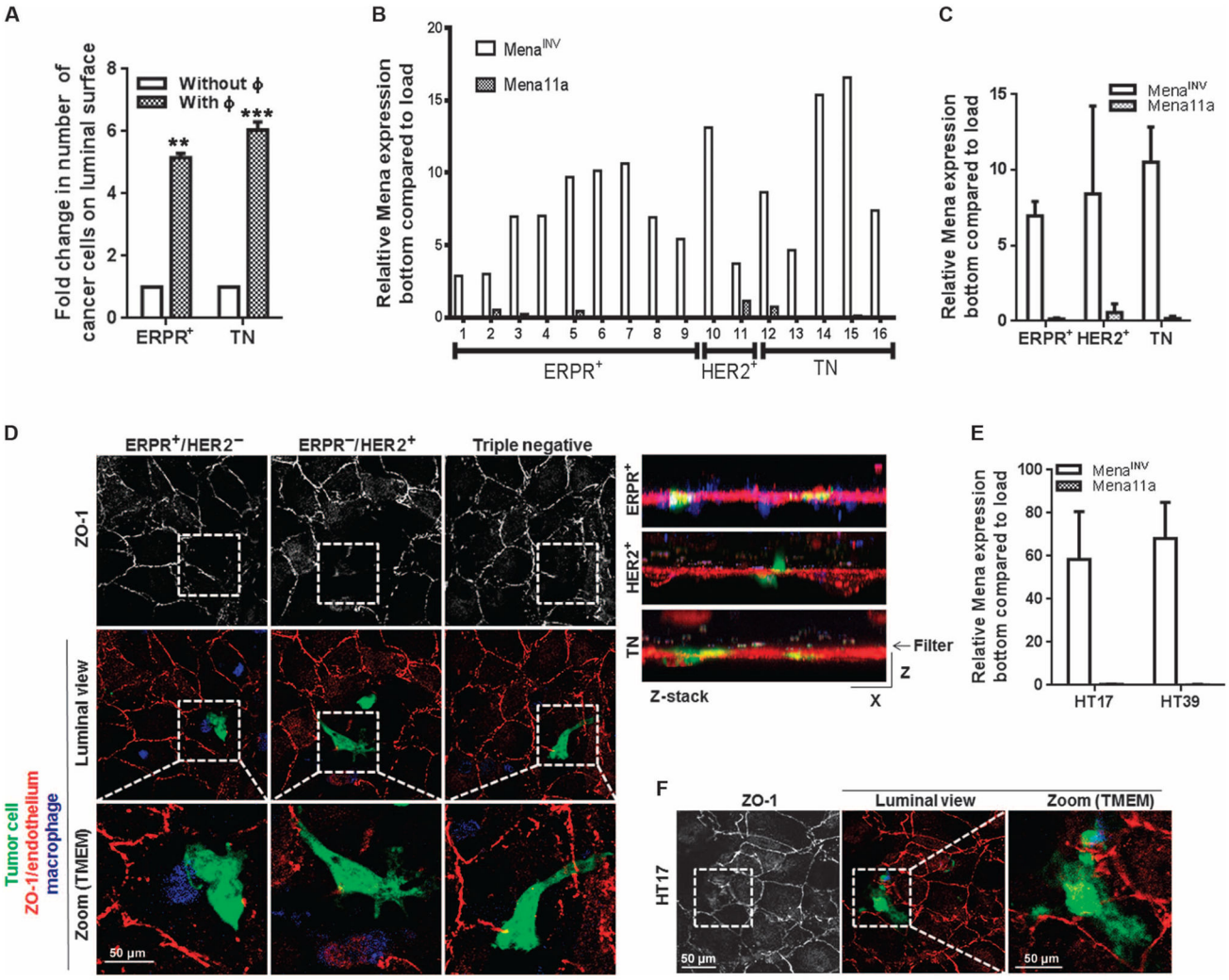

Fig. 4. iTEM assays using human patient IDC cells obtained from FNA biopsies

(**A**) Fold increase in the number of cells from ERPR$^+$ or TN cases that crossed a HUVEC monolayer in the presence of macrophages (Φ) relative to the number that crossed in the absence of macrophages. Data are means ± SEM from three experiments. $^{**}P < 0.005$, $^{***}P < 0.0005$, by two-tailed Student's *t* tests assuming equal variances. (**B**) Mena^{INV} or Mena11a transcript expression in cells that crossed the HUVEC monolayer relative to that in the loaded cell population. Data are from 16 patient cases. (**C**) Average Mena^{INV} and Mena11a isoform expression in iTEM-competent cells from (B) grouped by clinical subtype. Data were not significantly different by a Student's *t* test. (**D**) Apical z-sections from the iTEM assay. Tumor cells, green; macrophages, blue; HUVEC junctions (ZO-1), red. Squares indicate dissociating HUVEC junctions, magnified below. Right: Representative z-stacks by clinical subtype. Data are representative of each from the 16 cases in (B). (**E**) Mena^{INV} and Mena11a transcript expression in iTEM-competent cells from TN human tissue transplants HT17 and HT39. Data are means ± SEM from three mice each. (**F**) Apical z-sections of the iTEM assay with HT17 tumor cells as in (D). Images are representative of three experiments.

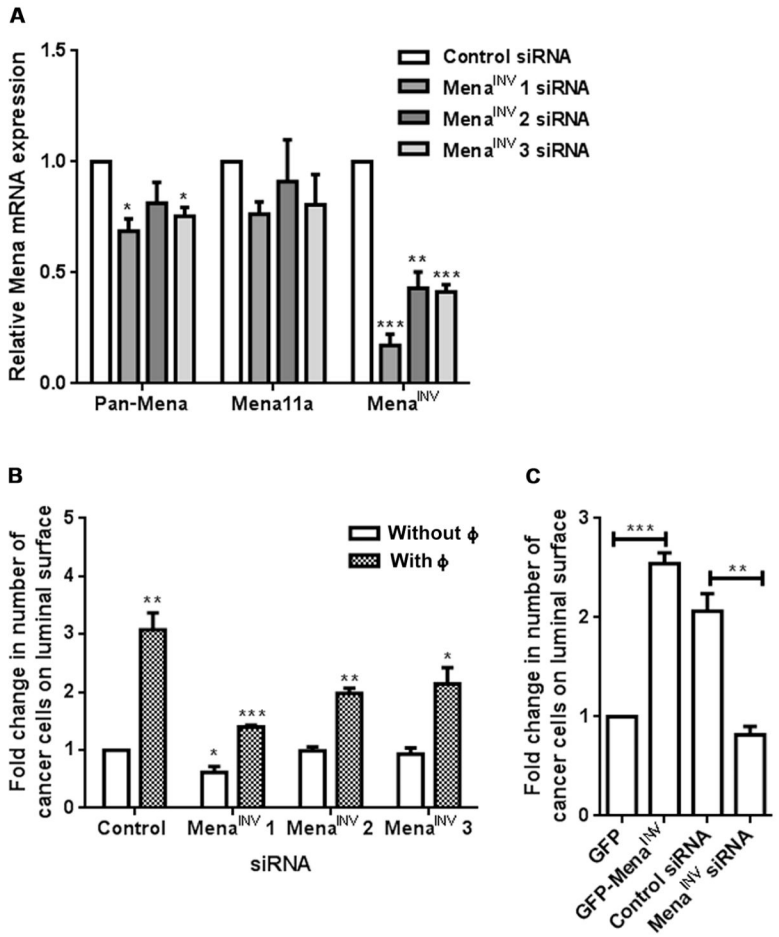

Fig. 5. Mena^{INV} is required for macrophage-induced iTEM in MDA-MB-231 TN breast cancer cells

(**A**) Transcript abundance for total Mena, Mena11a, and Mena^{INV} in parental MDA-MB-231 cells transfected with one of three Mena^{INV}-targeted siRNAs. (**B**) iTEM of MDA-MB-231 cells after Mena^{INV} depletion in the presence or absence of macrophages (Φ). (**C**) iTEM of MDA-MB-231 cells expressing GFP-tagged Mena^{INV}, alone or cotransfected with Mena^{INV}-targeted siRNA (1). iTEM was performed in the presence of macrophages. Data in (A) to (C) are means ± SEM from three experiments. **P* < 0.05, ***P* < 0.005, ****P* < 0.0005, by two-tailed Student's *t* tests assuming equal variances.

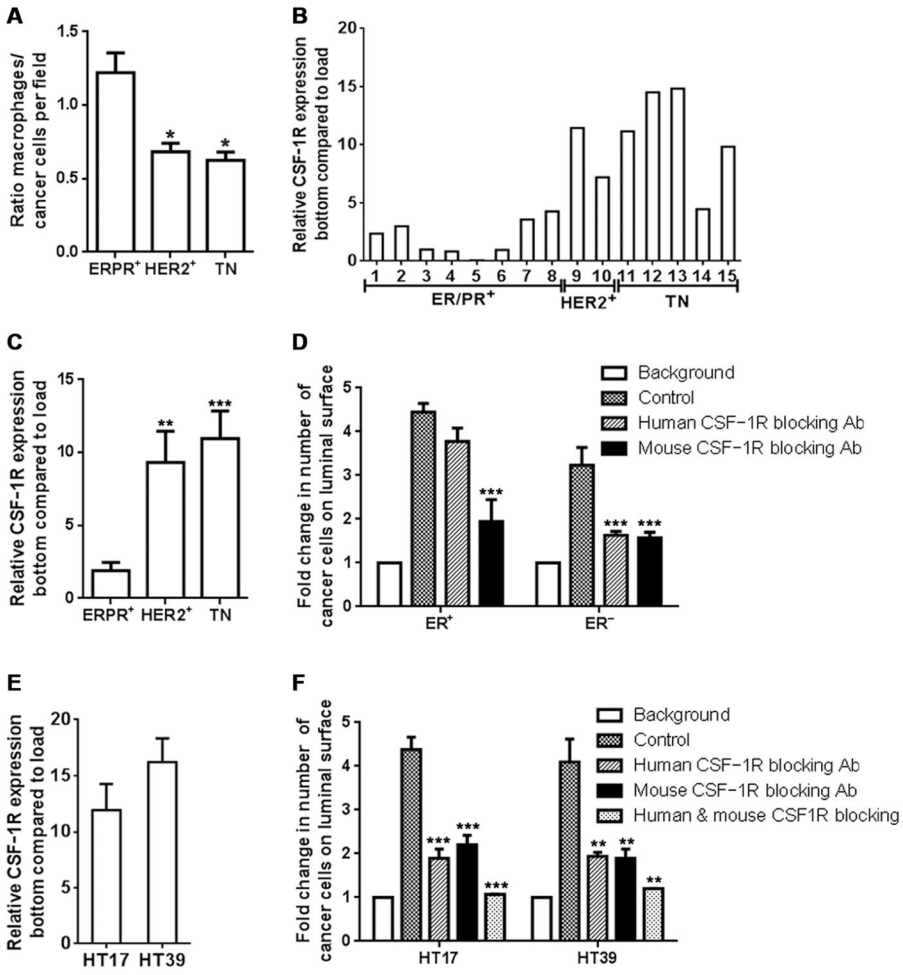

Fig. 6. *CSF1R* expression in iTEM-competent cells differs among breast cancer subtypes

(**A**) The number of macrophages associating with tumor cells during iTEM, presented as a ratio by clinical subtype. Data are means ± SEM from twelve 63× microscopic fields in two to three cases each. **P* < 0.05 compared with that in ERPR$^+$/HER2$^-$ cases. (**B** and **C**) *CSF1R* transcript abundance in iTEM-competent cells from each of 15 cases analyzed across clinical subtypes (B). Data in (C) are means ± SEM by clinical subtype shown in (B). (**D**) Effect of mouse-specific CSF-1R antibodies or human-specific CSF-1R antibodies on iTEM of ERPR$^+$/HER2$^-$, ERPR$^-$/HER2$^+$ (HER2$^+$), and TN cancers. Data are means ± SEM from three cases per subtype relative to the background (tumor cells cross without the presence of macrophages). Control, tumor cells cross in the presence of macrophages. (**E** and **F**) *CSF1R* transcript abundance in iTEM-competent cells from patient tumor transplants HT17 and HT39 (E), and the effect of mouse- or human-specific CSF-1R functionally blocking antibodies on iTEM capacity. Data are means ± SEM from five mice per tumor sample. ***P* < 0.005, ****P* < 0.0005. Statistical analyses in (A), (C), (D), and (F) used two-tailed Student's *t* tests assuming equal variances.

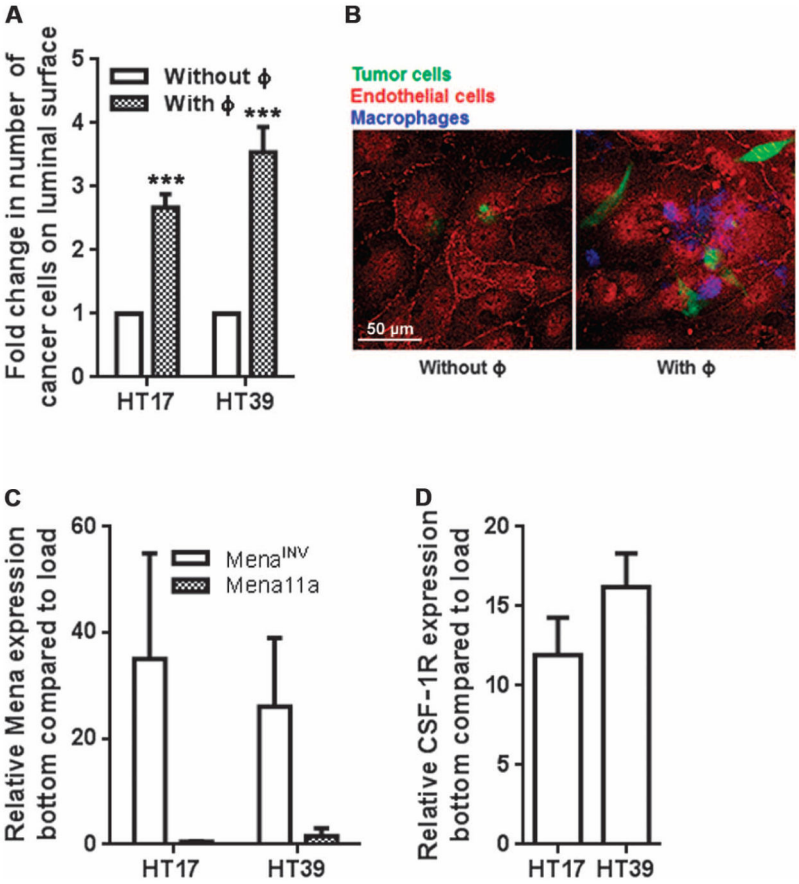

Fig. 7. Primary human macrophages increase iTEM of primary human breast cancer cells

(**A**) Number of iTEM-competent cells from TN human tissue transplants HT17 and HT39 in the presence or absence of primary human macrophages (Φ). (**B**) Representative apical z-sections of the iTEM assay demonstrating HT39 cells (green) and crossing the endothelial monolayer (red) in close proximity with macrophages (blue). (**C** and **D**) Relative Mena^{INV} and Mena11a (C) or CSF-1R (D) transcript abundance in iTEM-competent HT17 and HT39 cells in the presence of primary human macrophages. Data are means ± SEM from three mice for each tumor. ***$P < 0.0005$, two-tailed Student's *t* tests assuming equal variances.

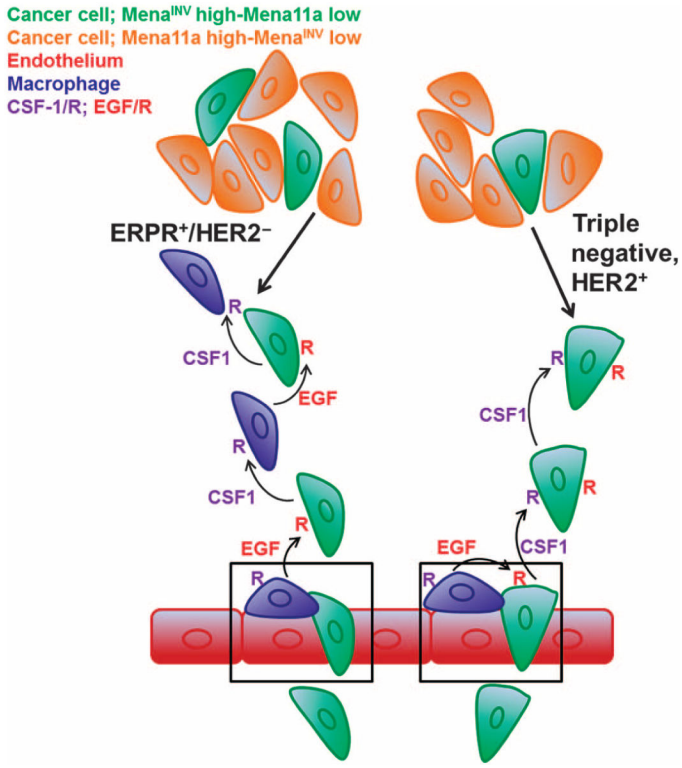

Fig. 8. Model of Mena^{INV}- and macrophage-mediated tumor cell invasion and TEM

ITEM-competent human breast cancer cells from all clinically relevant subtypes display Mena^{INV} high/Mena11a low isoform expression and perivascular macrophages promote endothelial transmigration at TMEM sites (outlined). iTEM in ERPR^{+}/HER2$^{−}$ cells is promoted by paracrine CSF-1–CSF-1R signaling, whereas iTEM in HER2^{+} and TN cells is promoted by both paracrine and autocrine CSF-1–CSF-1R signaling. R, receptor.